

Sign of Enhanced Three α Matter radius in $\alpha + {}^{12}\text{C}$ inelastic scattering

M. Tomita M. Iwasaki, R. Otani, M. Ito*

Department of Pure and Applied Physics, Kansai University

E-mail: itomk@kansai-u.ac.jp

Nuclear radius of three α rotational state in ${}^{12}\text{C}$ with a life time of 10^{-21} second, which has been expected to have much more extended radius than the ground ${}^{12}\text{C}$ nucleus, is speculated from systematic analysis of the differential cross section of the $\alpha + {}^{12}\text{C}$ inelastic scattering. Present analysis predicts about $0.6 \sim 1.0$ fm enhancement in the matter radius of the three α rotational state in comparison to the normal radius of the ground state. The spatial extension of the three α rotational state is comparable to the extended radius observed in the neutron halo phenomena. Constraint on the recent ab-initio calculation for the 3α states in ${}^{12}\text{C}$ is also discussed.

*The 26th International Nuclear Physics Conference
11-16 September, 2016
Adelaide, Australia*

*Speaker.

1. Introduction

Cluster structures, in which a nucleus is decomposed into several sub-units, are realized in the low excited states of light mass nuclei [1]. In the cluster structure, the sub-units are weakly coupled each other, and their matter radius is prominently extended in comparison to the radius of the ground state, which obeys the law of $\propto A^{1/3}$. In particular, such the enhancement of the matter radius is extensive in the 3α structure of the ${}^{12}\text{C}$ nucleus [2, 3]. The ground state of ${}^{12}\text{C}$ has a radius of 2.40 fm [2] with the spin-parity of 0^+ (0_1^+), while the excited 0_2^+ state at $E_x = 7.65$ MeV, which is called the Hoyle state, is considered to have a radius of 3.47 fm with the well developed 3α cluster structure [2]. The extension of the radius in 0_2^+ is predicted to be about 1 fm, which is comparable to the extension of the neutron halos discussed in ${}^{11}\text{Li}$ [4]. In this article, we propose a new method to obtain a signature of the enhanced matter radius of the 3α cluster state.

Unfortunately, a direct measurement of the radius of the Hoyle 0_2^+ states with the developed 3α cluster structure is impossible due to its short life time, but there are several attempts to get an evidence of the enhanced matter radius of the 3α Hoyle states from the inelastic scattering of ${}^{12}\text{C}$, which excites the Hoyle 0_2^+ state as a final state. In the inelastic scattering of light ions by ${}^{12}\text{C}$, which excites the ${}^{12}\text{C}(0_2^+)$ state in a final state, an oscillating pattern in the differential cross section of the scattered ion is discussed in connection to the enhanced radius of the final 0_2^+ state with the 3α structure [5, 6, 7, 8, 9]. However, the relation of the extended radius and the oscillating pattern of the cross section of the ${}^{12}\text{C}$ inelastic scattering still remains unclear [10, 11].

In the coupled-channel approaches [7, 8, 9], for example, nuclear interactions for the system of the ${}^{12}\text{C}$ target plus a projectile are constructed from the double folding model, which employs the internal wave function of ${}^{12}\text{C}$, obtained from the 3α resonating group method ($3\alpha\text{RGM}$) [2] and from an effective density-dependent nucleon-nucleon interaction. This coupled-channel calculation is called microscopic coupled-channels (MCC) [14]. Since the 3α RGM wave function can precisely describe the 3α structure in 0_2^+ , the constructed nuclear interaction in the 0_2^+ channel is more attractive at a surface region than the interaction in the ground channel. The MCC calculations employing the long-range 3α folding interaction have been applied to the $\alpha+{}^{12}\text{C}$ [7] and ${}^3\text{He}+{}^{12}\text{C}$ [8, 9] systems, and the calculation nicely reproduces the angular distributions of various exit channels. In the differential cross section for the 0_2^+ channel, a scattering angle for the first Airy minimum is shifted to the larger angle region, and the number of the Airy minima increases in a comparison to other inelastic channels, going to the rotational and vibrational states such as the 2_1^+ and 3_1^- states. From this result, the authors have claimed that the evolution of the Airy structure originated from the spatial extension of the nuclear interaction in the final 0_2^+ channel [7, 8, 9].

In the nuclear reaction, the final 3α states can be assessed through the transition from the incident ground channel, and the 3α state is observed as the final state in the reaction process. Therefore, a coupling potential, which induces a transition from the initial channel to the final channel, is expected as a main ingredient for the angular distribution of the inelastic scattering, and the distortion potential or the density distribution in the exit channel may be not so effective in comparison to the effect of the coupling potential. In fact, a dominance of the coupling potential in the inelastic scattering has been already pointed out by Takashina et al. [10, 11]. By employing the MCC calculation, which is the same method as in Refs. [7, 8, 9], the authors have clearly demonstrated that the Airy structure in the angular distribution is dominated by not the size of the

0_2^+ state, but by a spatial distribution of the coupling potential for the $0_1^+ \rightarrow 0_2^+$ transition.

Although the potential or density distribution in the final 3α channel itself plays a minor role in inelastic scattering, a coupling potential contains size information of the final 3α state because the coupling potential is determined by an overlap of the wave function between the initial ground state and the final 3α state. Therefore, an extended structure of the 3α state is indirectly reflected in the inelastic scattering to the 3α final state. We believe that it is still useful to consider a relation between an inelastic scattering and the internal size of the 3α structure. Recently, we have formulated the method of scattering radius, which can characterize a spatial size of the reaction area for the individual exit channels in a general exclusive reactions [12]. In this method, the angle-integrated cross section decomposed into each of the incident partial wave are used to measure the spatial size for the production area of the final channel. The validity of the scattering radius is checked for the monopole 0^+ excitation [12] but this method can be easily extended to general reaction channels.

In this article, we focus on the 2_2^+ state, which corresponds to the 3α rotational state of the Hoyle 0_2^+ state [2, 3] with a life of 10^{-21} sec. (width of $\Gamma \sim 1$ MeV) and the method of the scattering radius is applied. We will demonstrate that a direct evidence of the enhanced matter radius in the 2_2^+ state clearly appears in the $\alpha + {}^{12}\text{C}$ inelastic scattering. In a modern theory, the Hoyle rotational 2_2^+ state, which has been recently identified in experiment [13], is interpreted in terms of an α halo state with a dilute 3α structure [3]. The differential cross section of $\alpha + {}^{12}\text{C}(0_1^+) \rightarrow \alpha + {}^{12}\text{C}(2_2^+)$ is compared with the reference reaction of $\alpha + {}^{12}\text{C}(0_1^+) \rightarrow \alpha + {}^{12}\text{C}(2_1^+)$, in which the 2_1^+ state is a rotational state of the ground 0_1^+ state with a spatially compact structure. In the inelastic scattering to the $2_{1,2}^+$ states, the kinematic conditions are completely democratic but only the matter radii are prominently different, say 2.4 fm for 2_1^+ and 4.0 fm for 2_2^+ [2]. Thus, the comparison of these two inelastic scattering is expected to give the evidence of the extended matter radius of the 2_2^+ state, which involves the 3α cluster structure. We apply the method of the scattering radius to the exit channels of $2_{1,2}^+$ and try to speculate the lower bound of the matter radius of the 3α rotational state, the 2_2^+ state.

2. Theoretical Framework

We calculate the differential and partial cross sections of an α particle scattered by ${}^{12}\text{C}$ in the formulation of the microscopic coupled-channels (MCC) calculation [7, 8, 14]. In MCC framework, we solve a set of the coupled-channel equation for the $\alpha-{}^{12}\text{C}$ system, which is given in the symbolic form

$$(T_f(\mathbf{R}) + V_{f,f}(\mathbf{R}) - E_f)\chi_f(\mathbf{R}) = -\sum_{i \neq f} V_{f,i}(\mathbf{R})\chi_i(\mathbf{R}). \quad (2.1)$$

Here the subscripts of f and i design a channel. In the case of the spinless incident channel, such as $\alpha + {}^{12}\text{C}(0^+)$, the coupled-channel equation is solved in a subspace of the incident orbital spin of L . In Eq. (2.1), $T_f(\mathbf{R})$ represents the kinetic energy of the relative motion of the $\alpha-{}^{12}\text{C}$ system with a relative coordinate \mathbf{R} , while $V_{f,i}(\mathbf{R})$ denotes the coupling potential for the transition from channel i to channel f . The total energy in the channel f , E_f , is given by the relation of $E_f = E - \varepsilon_f$ with the α incident energy E and the ${}^{12}\text{C}$ internal energy of ε_f . $\chi_f(\mathbf{R})$ is the $\alpha-{}^{12}\text{C}$ relative wave function for the channel f , which should be solved in the coupled-channel equation.

$V_{f,i}(\mathbf{R})$ denotes the coupling potential for the transition of $i \rightarrow f$ in ${}^{12}\text{C}$, which is calculated from the double folding model. The coupling potential calculated from the double folding procedure is symbolically written as

$$V_{f,i}(\mathbf{R}) = N_R \int \int \rho_{f,i}^{({}^{12}\text{C})}(\mathbf{r}_1) \rho^{(\alpha)}(\mathbf{r}_2) v_{NN}(\mathbf{s}) d\mathbf{r}_1 d\mathbf{r}_2 \quad (2.2)$$

with $\mathbf{s} = \mathbf{r}_2 - \mathbf{r}_1 - \mathbf{R}$. Here \mathbf{r}_1 (\mathbf{r}_2) denotes a coordinate measured from the center of mass in the ${}^{12}\text{C}$ (α) nucleus. $\rho_{f,i}(\mathbf{r})$ represents the diagonal ($f = i$) or transition ($f \neq i$) densities of ${}^{12}\text{C}$, which are calculated by the microscopic 3α cluster model, resonating group method (RGM) [2], while $\rho^{(\alpha)}(\mathbf{r})$ denotes the density of α particle, which reproduce the charge form factor of the electron scattering. In Eq. (2.2), v_{NN} represents the effective nucleon-nucleon (NN) interaction which acts between a pair of nucleon contained in the ${}^{12}\text{C}$ nucleus and the α particle. In the present calculation, we adopt the DDM3Y (Density Dependent Michigan 3-range Yukawa) interaction [15].

The normalization factor N_R is introduced because the folding potential contains ambiguity in its strength. This ambiguity arises from the neglect of the anti-symmetrization effect between the projectile and the target except for the knockon exchange [16]. Here this factor is set to $N_R = 1.42$ over all the α incident energy, which is consistent to the MCC calculation in Ref. [7, 8]. In the α scattering, the double folding potential needs a considerably large N_R , say about 1.3 as pointed out in the first application of DDM3Y to the α scattering [15]. This modification in the potential strength is originated from the violation of density saturation of an α particle. The improvement of the double folding potential for the α scattering has recently been discussed in Ref. [17].

In addition to the folding potential, we introduce the absorptive potential with the Saxon-Woods form factor in the diagonal ($f = i$) transition in order to simulate other reaction process, and the parameter set of Saxon-Woods is tuned so as to reproduce all of the observed differential cross sections as much as possible. As for the internal excitation of ${}^{12}\text{C}$, we include the low-lying collective states (2_1^+ and 3_1^-) and the 3α cluster states (0_2^+ , 0_3^+ , 2_2^+) in addition to the ground 0_1^+ state.

3. Results

We have solved the coupled-channels equation, which is given in Eq. (2.1), for the $\alpha + {}^{12}\text{C}$ scattering at $E_\alpha = 386$ MeV [13] with the nuclear interaction in Eq. (2.2). The MCC calculation reproduce the differential cross sections of the scattering to 0_1^+ , 2_1^+ , 3_1^- states. Furthermore, the theoretical calculation nicely reproduce the inelastic scattering to the excited state observed at $E_x \sim 10$ MeV, which is considered as the incoherent mixture of 0^+ and 2^+ strength in the experiment, by taking the summation of the differential cross sections of the 0_3^+ and 2_2^+ states.

A comparison of the 2_1^+ cross section (dotted curve) and the 2_2^+ one (solid curve) is shown in Fig. 1 (left panel). The peak position of the 2_2^+ cross section (solid curve) shifts to the forward angular region, and its angular distribution has the shrinkage and rapid fall-down structure in comparison to the 2_1^+ cross section (dotted curve). The shift and shrinkage features are completely consistent to the result of the multi-pole decomposition analysis (MDA) of the experimental cross section, which is performed in the range of $\theta_{c.m.} < 15^\circ$ [13].

In order to analyze the difference of the differential cross sections shown in the left panel of Fig. 1 more deeply, we have performed the partial wave analysis, in which the angle-integrated

cross sections of the left panel are decomposed into the individual components of the incident orbital spin L . The individual components of the angle integrated cross sections for the transition from the ground 0_1^+ state to the final state (f) are called the partial cross section, $\sigma(L, f)$.

The results of the partial wave decomposition are shown in the right panel of Fig. 1. The open circles show the partial wave distribution (L -distribution) of the angle-integrated 2_1^+ cross section ($\sigma(L, 2_1^+)$), while the L -distribution of 2_2^+ is plotted by the solid circles ($\sigma(L, 2_2^+)$).

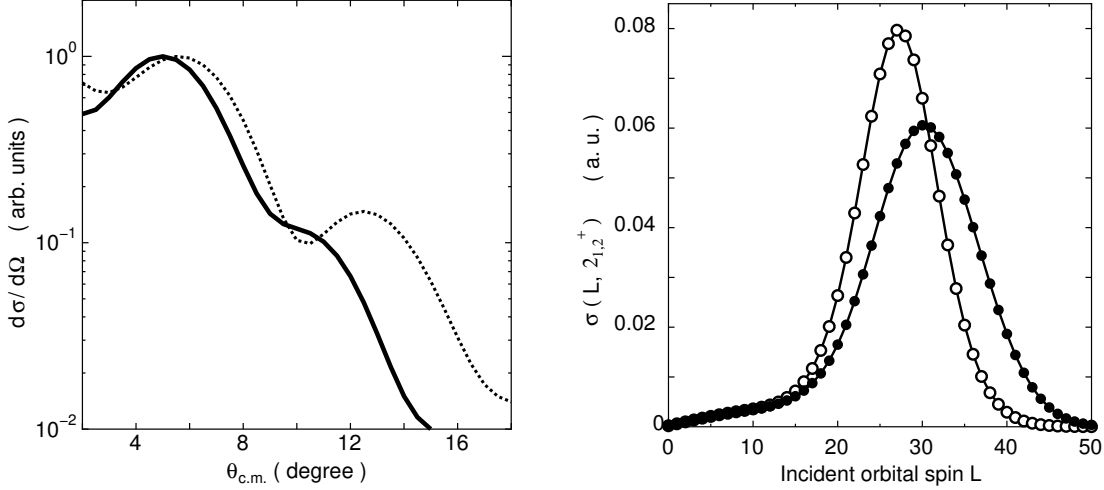


Figure 1: Left panel: Theoretical differential cross sections of the final state of 2_1^+ (dotted curve) and 2_2^+ (solid curve) in the $\alpha + {}^{12}\text{C}$ inelastic scattering. The magnitudes of both the cross sections are normalized by the maximum value around $\theta_{c.m.} \sim 5^\circ$. Right panel: Partial wave decomposition of the angle integrated cross sections calculated as the function of the incident orbital spin L (L -distribution). The open and solid circles show the partial cross sections of the 2_1^+ and 2_2^+ final states, respectively. The magnitudes of all the partial cross section is normalized by the total cross section, which is the summations of the partial cross sections.

In the comparison of $\sigma(L, 2_1^+)$ with $\sigma(L, 2_2^+)$, we can clearly see the extended L -distribution of 2_2^+ to the higher L region. This extension of 2_2^+ in the L -space (right panel) is just opposite to the shrinkage in the θ -space, the differential cross section (left panel). This is nothing but the uncertainty relation of $\Delta L \cdot \Delta\theta \sim 1$, which can be hold in the diffraction scattering. According to the classical relation of $L = kb$, where k and b denote the incident wave number and the impact parameter, respectively, the extension of the L -distribution in the right panel of Fig. 1 clearly means that the production area of the 2_2^+ state is more extended than the area of the 2_1^+ production.

The distribution in the L -space can be transformed into a size of the production area of the final state by applying the method of the scattering radius [12]. In this method, the effective orbital spin \bar{L} for the transition of $0^+ \rightarrow 2_{1,2}^+$ is derived according to the following expression:

$$\bar{L}(2_i^+) = \sqrt{\frac{\sum_L \hat{L}^4 \sigma(L, 2_i^+)}{\sum_L \hat{L}^2 \sigma(L, 2_i^+)}} \quad (i = 1, 2) \quad (3.1)$$

with a definition of $\hat{L} = \sqrt{L(L+1)}$. The radius of the final-state production, which is called the scattering radius (R_{SC}), is simply obtained according to the classical relation of $\bar{L} = kR_{SC}$. R_{SC} naturally goes to the matter radius of a target nucleus in the high energy limit of the proton elastic scattering [6, 12, 18].

Table 1: Effective orbital spins \bar{L} and the scattering radius R_{SC} calculated from the definition in Eq. (3.1). The theoretical mean radius of the density distribution (\bar{r}) for the 2_1^+ ($E_x = 4.44$ MeV) and 2_2^+ ($E_x = 10.30$ MeV) states are also shown in the right-most column [2].

State	E_x (MeV)	\bar{L}	R_{SC} (fm)	\bar{r} (fm)
2_1^+	4.44	29.67	4.58	2.38
2_2^+	10.3	33.69	5.20	4.00

The results of \bar{L} and R_{SC} for the 2_1^+ and 2_2^+ states are summarized in table 1. The calculated effective orbital spin \bar{L} is slightly shifted to the higher value than the peak position of the L -distribution, $\sigma(L, 2_{1,2}^+)$ in the right panel of Fig. 1 because of the finite width in their distribution. The resultant scattering radius for 2_1^+ is $R_{SC}(2_1^+) = 4.58$ fm, while the radius for 2_2^+ is $R_{SC}(2_2^+) = 5.20$ fm. The obtained R_{SC} are larger than the root-mean-squared radius (\bar{r}) of the 2_1^+ and 2_2^+ states (2.38 fm and 4.00 fm) [2]. One should notice that there is no meaning in the magnitude of R_{SC} itself because the magnitude of R_{SC} strongly depends on the definition of \bar{L} in Eq. (3.1). Thus, we should focus on the relative difference of R_{SC} between 2_1^+ and 2_2^+ . The difference of the scattering radius is $\Delta R_{SC} = R_{SC}(2_2^+) - R_{SC}(2_1^+) = 0.62$ fm, while the difference of \bar{r} in the structure calculation is $\Delta r = \bar{r}(2_2^+) - \bar{r}(2_1^+) = 1.62$ fm. The enhancement in R_{SC} is smaller than that in \bar{r} , and the reduction of ΔR_{SC} will be discussed in the later part.

We have extended the MCC calculation with the method of the scattering radius to the lower α incident energy of $E_\alpha \leq 240$ MeV. In the lower energy region, unfortunately, there is no experimental data on the excited state at $E_x \sim 10$ MeV, which contains the 2_2^+ component. Therefore, the parameters of the absorptive potential of the 3α cluster states (0_2^+ , 0_3^+ , 2_2^+) are set to a common value, and the parameters are tuned so as to reproduce the cross section of 0_2^+ (and 0_3^+) as much as possible. In all the energy region considered, ΔR_{SC} ranges from 0.6 fm to 1 fm, which means that $R_{SC}(2_2^+)$ is larger than $R_{SC}(2_1^+)$ over the entire incident energy. The enhancement of $R_{SC}(2_2^+)$ is equivalent to the fact that the differential cross section of the 2_2^+ state is more shrunk than that of the 2_1^+ state.

From the systematic values of ΔR_{SC} , we can speculate the lower bound of the matter radius of the 2_2^+ state. In a naive consideration, we can image the relation of ΔR_{SC} and the matter radius R_m , such as

$$R_m(2_2^+) \geq R_m(2_1^+) + \Delta R_{SC} . \quad (3.2)$$

In the present analysis, $\Delta R_{SC} \sim 1$ fm is predicted in the lower energy region of $E_\alpha \leq 240$ MeV. The matter radius of 2_1^+ is still unknown but we can safely assume $R_m(2_1^+) \sim R_m(0_1^+)$. This assumption

is because the 2_1^+ state is the first excited state of the ground 0_1^+ state and hence, we can expect that the spatial size of 2_1^+ is not drastically changed from the size of the ground 0_1^+ . This assumption is also supported by the 3α RGM calculation [2]. Therefore, the matter radius of the Hoyle rotational state is speculated to $R_m(2_2^+) \geq 3.7$ fm if we employ the experimental value of $R_m(0_1^+) = 2.7$ fm [19].

4. Summary and discussions

In summary, we have shown that the enhanced radius of the 2_2^+ state can be probed via the differential cross section by comparing with the respective cross section of the 2_1^+ state. The inelastic differential cross section of the 2_2^+ state is more shrunk than that of the 2_1^+ state, and this shrinkage is a first evidence of the extended matter radius of the final 2_2^+ state in the inelastic scattering of $\alpha + {}^{12}\text{C}(0_1^+) \rightarrow \alpha + {}^{12}\text{C}(2_2^+)$. According to the prescription of the partial wave decomposition, the partial wave components of the cross sections are converted into the scattering radius, which characterizes a size of the reaction area for the final state production. According to the evaluation of the scattering radius, the shrunk structure of the differential cross section corresponds to about $0.6 \sim 1$ fm enhancement in the size of the production area of the final 2_2^+ state.

Enhancement of R_{SC} ($\Delta R_{SC} \sim 1$ fm) is smaller than the difference of the respective root-mean-squared radius ($\Delta \bar{r} \sim 1.6$ fm), which is predicted by the structure calculation [2]. This is because of the feature of the inelastic scattering. As pointed out in Refs [10, 11], the inelastic scattering going to the excited states are dominated by the size of the coupling potential, which induces the transition from the incident 0_1^+ state to the final $2_{1,2}^+$ state. Thus, the inelastic scattering cannot probe the size of the density (or potential) in the final state completely, and the R_{SC} values obtained from the inelastic scattering is considered to underestimate the true enhancement of the matter radius in the final state. However, we believe that about 1 fm in the difference of R_{SC} is still meaningful enhancement.

About 1 fm enhancement in the matter radius of the Hoyle rotational state is comparable to the extended radius in ${}^{11}\text{Li}$ [4], which largely deviates from the systematics of $\propto A^{1/3}$. ${}^{11}\text{Li}$ corresponds to the excited state from ${}^{11}\text{B}$, in which the isospin degrees of freedom is excited. The excitation energy of ${}^{11}\text{Li}$, ($\text{B.E.}({}^{11}\text{Li}) - \text{B.E.}({}^{11}\text{B})$) is about 34 MeV, while the excitation energy of ${}^{12}\text{C}(2_2^+)$ is just about 10 MeV. Thus, the 1 fm enhancement of the matter radius in ${}^{12}\text{C}(2_2^+)$ is exotic phenomena, which occurs in much lower excitation energy than the neutron-excess nucleus.

Furthermore, the identification of 1 fm enhancement imposes a strong constraint on the recent ab-initio calculation which seems to reproduce the excitation energy of the Hoyle 0_2^+ and 2_2^+ states [20]. In this structure calculation, the matter radius of the Hoyle rotational 2_2^+ state is almost same as the radius of the ground state (2.4 fm) [20], which is much smaller than the prediction by the 3α cluster model (~ 4.0 fm) [2, 3]. In previous studies, there was no information about the matter radius of the excited states that should be compared with the theoretical calculation. Therefore, the speculation of the lower bound of the matter radius of the Hoyle rotational 2_2^+ state from the experimental observables is quite important in future studies. Since the experimental information of the differential cross section of the 2_2^+ state is still insufficient, the measurement of the differential cross section of the excited state at $E_x \sim 10$ MeV and careful MDA to separate the 2_2^+ component should be extended over a wide angle and energy region.

Finally, let us discuss the new insight in the present approach. The comparison of the yrast 2_1^+ state and the Hoyle rotational 2_2^+ state is a new insight in the discussion of the inelastic scattering of ${}^{12}\text{C}$, which was absent in the previous studies about relation of the matter radius and the inelastic scattering to the Hoyle 0_2^+ state [5, 6, 7, 8, 10, 11]. In the case of 0_2^+ excitation, the enhancement of the matter radius of the final 0_2^+ state may be reflected in the differential cross section but it is difficult to extract an evidence only from the cross section of the 0_2^+ state. The anomalous feature in the 0_2^+ cross section should be identified from the comparison with a certain kind of "reference reactions". In a naive consideration, the elastic scattering of the 0_1^+ state seems to be an appropriate reference that is compared to the 0_2^+ channel. However, the elastic channel is completely inappropriate as the reference reaction channel because the elastic and inelastic scattering occur in the different reaction process; the former is basically dominated by the diagonal potential of the ground 0_1^+ channel, while the latter is induced by the coupling potential. In the vicinity of the 0_2^+ state, there is no excited 0^+ state with the yrast (or spatially compact) structure, which must be compared to 0_2^+ and hence, the identification of the enhancement in 0_2^+ is quite difficult. On the contrary, in the case of the inelastic scattering to the 2^+ state, there is a pair of the 2^+ channels, such as the yrast 2_1^+ channel and the excited 2^+ one, which can be compared directly.

The comparison of the same (finite) spin-parity states excited by the inelastic scattering is essential in the present analysis. The similar comparison of the yrast state and the cluster state can be generalized to other nuclei because a cluster state with a finite spin always appear above the respective yrast state with a compact shell model like structure. Therefore, it is very interesting to apply the present method to other cluster systems. An interesting application is the ${}^{10}\text{Be}$ nucleus. In this nucleus, the intrinsic structure can be nicely described by the covalent (or molecular) orbit structure of two valence neutron around the two center cores of ${}^8\text{Be} = \alpha + \alpha$ [21]. The yrast 2_1^+ and the excited 2_2^+ state have the spatially compact structure, while the 2_3^+ state is considered to have the well developed structure of $\alpha + \alpha + N + N$, in which two neutrons form the covalent σ^+ orbital [21]. Therefore, the comparison of the $2_{1,2}^+$ state and the 2_3^+ state is very interesting to identify the developed 2α cluster structure with the σ^+ orbital. The calculation of the $\alpha + {}^{10}\text{Be}$ inelastic scattering is now underway.

References

- [1] K. Ikeda et al., *Prog. Theor. Phys.* **68**, 1 (1980).
- [2] Y. Fukushima and M. Kamimura, *Proceedings of the International Conference Nuclear Structure*, J. Phys. Soc. Jpn. **44**, 225 (1977); M. Kamimura, *Nucl. Phys. A* **351**,456 (1981).
- [3] Y. Funaki, A. Thosaki, H. Horiuchi, P. Schuck, and G. Reöpke, *Eur. Phys. J. A* **24**, 321-342 (2005), and references therein.
- [4] I. Tanihata, H. Savajolos, R. Kanungo, *Prog. Part. Nucl. Phys.* **68**, 215 (2013).
- [5] A. N. Danilov, T. L. Belyaeva, A. S. Demyanova, S. A. Ganchalov, and A. A. Ogloblin, *Phys. Rev. C* **80**, 054603 (2009).
- [6] K. Iida, S. Koide, A. Kohama, and K. Oyamatsu, *Mod. Phys. Lett. A* **27**, 1250020 (2012).
- [7] S. Ohkubo and Y. Hirabayashi, *Phys. Rev. C* **70**, 041602(R) (2004).
- [8] S. Ohkubo and Y. Hirabayashi, *Phys. Rev. C* **75**, 044609 (2007).

- [9] Sh. Hamada, Y. Hirabayashi, N. Burtbayev, and S. Ohkubo, *Phys. Rev. C* **87**, 024311 (2013).
- [10] M. Takashina and Y. Sakuragi, *Phys. Rev. C* **74**, 054606 (2006).
- [11] M. Takashina, *Phys. Rev. C* **78**, 014602 (2008).
- [12] M. Tomita, M. Iwasaki, R. Otani, M. Ito, *Phys. Rev. C* **89**, 034619 (2014).
- [13] M. Itoh et al., *Phys. Rev. C* **84**, 054308 (2011).
- [14] M. Ito, Y. Hirabayashi, and Y. Sakuragi, *Phys. Rev. C* **66**, 034307 (2002), and references therein.
- [15] A.M. Kobos, B.A. Brown, P.E. Hodgson, G.R. Satchler, A. Budzanowski, *Nucl. Phys. A* **384**, 65 (1982).
- [16] T. Wada, H. Horiuchi, *Prog. Theor. Phys.* **80**, 502 (1988), and references therein.
- [17] K. Egashira, K. Minomo, M. Toyokoawa, T. Matsumoto, M. Yahiro, *Phys. Rev. C* **89**, 064611 (2014).
- [18] A. Kohama, K. Iida, and K. Oyamatsu, *J. Phys. Soc. Jpn.* **85**, 094201 (2016), and references therein.
- [19] J. C. Kim, R. S. Hicks, R. Yen, I. P. Auer, H. S. Caplan, and J. C. Bergstrom, *Nucl. Phys. A* **297**, 301 (1978).
- [20] E. Epelbaum, H. Krebs, T. A. Lähde, D. Lee, Ulf-G. Meißner, *Phys. Rev. Lett.* **109**, 252501 (2012), and references therein.
- [21] M. Ito and K. Ikeda, *Rep. Prog. Phys.* **77**, 096301 (2014), and references therein.